ACS APPLIED MATERIALS & INTERFACES

Research Article

www.acsami.org

Bilayer Mass Transport Model for Determining Swelling and Diffusion in Coated, Ultrathin Membranes

Nichole K. Nadermann, Edwin P. Chan,* and Christopher M. Stafford*

Materials Science and Engineering Division, National Institute of Standards and Technology, 100 Bureau Drive, MS 8542, Gaithersburg, Maryland 20899, United States

Supporting Information

ABSTRACT: Water transport and swelling properties of an ultrathin, selective polyamide layer with a hydrophilic polymer coating, i.e., a polymer bilayer, are studied using quartz crystal microbalance with dissipation (QCM-D). Specifically, QCM-D is used to measure the dynamic and equilibrium change in mass in a series of differential sorption experiments to determine the dependence of the apparent diffusion coefficient and equilibrium swelling of the bilayer as a function of the water vapor activity. To determine transport properties specific to the polyamide layer, sorption kinetics of the bilayer was modeled with a bilayer mass transport model. The swelling and water diffusion coefficients are interpreted according to the Painter−Shenoy polymer network swelling model and the solution-diffusion model, respectively.

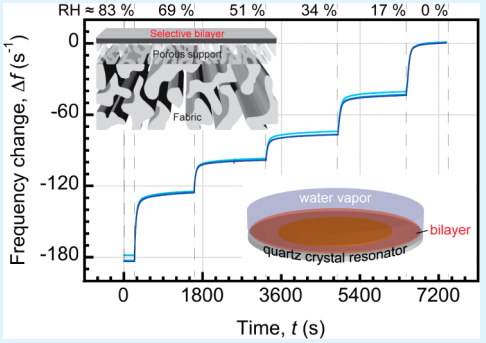

KEYWORDS: *bilayer mass transport, desalination, diffusion, polyamide*

1. INTRODUCTION

Water desalination via reverse osmosis (RO) is the most efficient commercial technology for providing clean water supplies and is expected to play an increasingly critical role in the coming decades.[1,2] Commercial RO membranes typically consist of a thin, selective polyamide (PA) membrane reinforced by a porous polysulfone layer and a nonwoven polyester fabric, which are incorporated as mechanical support against applied pressures during operation (schematically shown in Figure 1a). The PA selective layer is fabricated via interfacial polymerization (IP), which produces an ultrathin membrane (≈100−200 nm) with a very rough surface morphology (root mean square roughness ≈100 nm). Not only is the film rough, the anterior side of the PA selective layer is often coated with a hydrophilic polymer coating to improve wettability and minimize fouling.[3,4] These thin-film composite (TFC) membranes are designed for efficient water desalination, i.e., the highest water/salt selectivity and water flux with the lowest energy footprint.

Understanding transport within the PA selective layer is critical for developing next-generation water desalination membranes, as this is the sole layer that discriminates salt ions from water and serves as the bottleneck for total flux. The solution-diffusion model, the most widely accepted model of transport in RO membranes,[5] states that water flux (J) is related to the water diffusion coefficient in the membrane (D), membrane thickness (h), and volume fraction of water (ϕ) as follows:

$$J = D\frac{\phi_0 - \phi_h}{h\phi_0^{2/3}} \quad (1)$$

The subscripts "0" and "h" refer to the feed and permeate sides of the selective layer, respectively. The term $(\phi_0 - \phi_h)/\phi_0^{2/3}$ describes the water concentration profile in the membrane. From eq 1, it can be seen that the efficiency of a membrane can be characterized by the swollen membrane thickness and diffusion coefficient.

A variety of techniques exist for measuring swelling and transport in polymers, though few are suitable for the RO membrane studied in this work. Swelling in polymers can be measured via gravimetric,[6,7] microscopy,[8,9] scattering,[10,11] reflectivity,[6,12] and optical[13,14] techniques. Several of these same techniques, including gravimetry-,[15,16] impedance-,[17] optical-,[7,18] and spectroscopy[19−23]-based measurements, have been used for characterizing solvent diffusion in polymeric materials. A recent review by Bernstein et al.[24] provides details on experimental techniques that can be used to characterize swelling and transport in membranes. However, the surface roughness resulting from IP prohibits or complicates the use of scattering, reflectivity, and optical techniques. Additionally, the time scale of diffusion ($\sim h^2/D$) for the ultrathin desalination membrane studied in this work limits available characterization methods to only certain gravimetric techniques (including the one discussed in this paper).

Quartz crystal microbalance (QCM) has long been a popular gravimetric technique for studying sorption in ultrathin layers because of its nanogram sensitivity, high sampling rate, and variety of atmospheres in which it can be used (including in

Received: October 14, 2014
Accepted: January 19, 2015
Published: January 19, 2015

DOI: 10.1021/am507091s
ACS Appl. Mater. Interfaces 2015, 7, 3492−3502

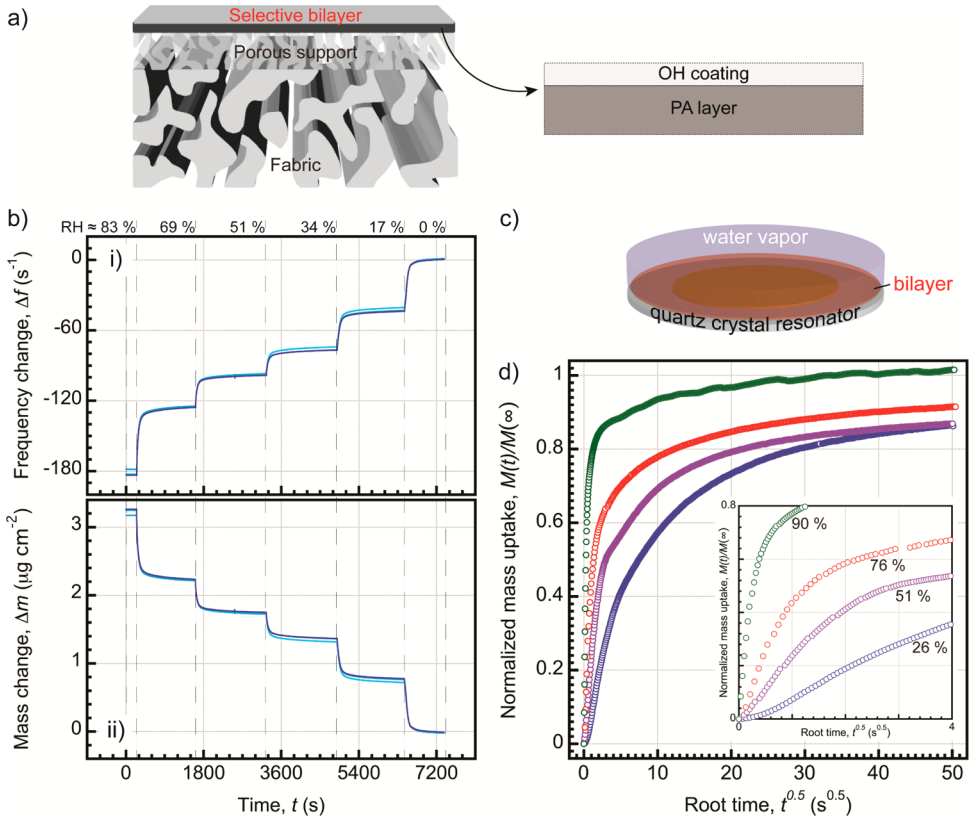

Figure 1. (a) Schematic of the thin film composite reverse osmosis membrane. The selective bilayer consists of a polyamide selective layer (PA layer) coated with a hydrophilic polymer coating (OH-coating). (b) Representative differential desorption data of the OH-coated PA bilayer measured by QCM-D. (i) The change in resonance frequency (Δf) versus time (t) due to changes in relative humidity (RH). (ii) The calculated change in the mass (Δm) of the bilayer based on the Sauerbrey model. The multiple data sets correspond to the different resonance modes or overtones (n = 3, 5, 7) of the sensor. (c) The illustration shows the geometry of the sample environment of the water vapor desorption study. (d) Change in normalized mass due to a steplike reduction in RH for four different initial relative humidity levels (26%, 51%, 76%, and 90% RH) versus the square root of time, $t^{1/2}$. The inset shows the initial change in the mass where the water diffusion coefficients are extrapolated.

vacuum, humidity, and liquid).[16] QCM with dissipation (QCM-D) is a derivative technique that independently measures the rate of energy dissipation in a sample and can be used to quantify the influence of membrane roughness on sorption measurements.[25] These attributes make QCM-D suitable for measuring minute changes of water absorbed and desorbed by thin polymer layers.[26] While QCM-D has been utilized for studying polymer thin layers,[11,12,27] it has not been used to measure the transport properties of RO membranes.

In this work, QCM-D is demonstrated as a measurement technique for capturing the desired transport properties of the selective PA layer. The water diffusion coefficient and swelling of a coated commercial PA membrane is characterized by measuring the time-dependent and equilibrium water sorption of the membrane as a function of relative humidity. One complication in measuring sorption and diffusion of water in commercial membrane selective layers is the near-ubiquitous presence of a hydrophilic polymer (OH) coating that is added on top of the polyamide active layer to increase hydrophilicity and to reduce fouling. To deconvolute water transport in the OH-coating from the PA layer, we present a bilayer mass transport model that provides insight into sorption kinetics within individual layers of a bilayer system. The model is material agnostic and can be used with other measurement techniques that provide mass or concentration data, such as infrared spectroscopy or ellipsometry. Finally, we consider the implications of humidity-dependent diffusion coefficients and swelling in the context of the solution-diffusion model.

2. MATERIALS AND METHODS

Reverse Osmosis (RO) Membrane. The commercial RO membrane studied in this work was kindly provided by Dow FilmTec [sea water high rejection (SWHR) membrane, Dow FilmTec, Edina, MN]. The selective PA layer is fully aromatic and is produced via IP of trimesoyl chloride (TMC) and *m*-phenylenediamine (MPD). The presence of an OH-coating was indicated by polarization modulation infrared reflection adsorption spectroscopy (PM-IRRAS, Thermo-Fisher) as well as with transmission electron microscopy (TEM, Phillips EM400T) imaging. This is consistent with the findings of Tang et al.,[3] in which TEM and spectroscopy were used to characterize several commercial membranes, including the SWHR membrane. The results from PM-IRRAS and TEM are included in the Supporting Information (SI).

A bilayer consisting of a selective PA membrane and an OH-coating was separated from the two mechanical support layers [polyester and polysulfone (PSF)] using a procedure described previously,[28] which we will only discuss briefly here. First, the thick polyester layer was manually peeled off of a TFC coupon that was adhered to a glass substrate. The remaining three-layer structure consisting of PSF, PA, and the OH-coating was cut into a ≈1 cm diameter circle. This circular sample was placed onto a cleaned quartz crystal sensor wetted with dimethylformamide (DMF) such that the OH-coating is in contact with the sensor and the PSF layer is exposed to atmosphere. Prior to depositing the sample, the sensors were cleaned using ultraviolet (UV)−ozone for 10 min; placed in a solution of hydrochloric acid,

DOI: 10.1021/am507091s
ACS Appl. Mater. Interfaces 2015, 7, 3492−3502

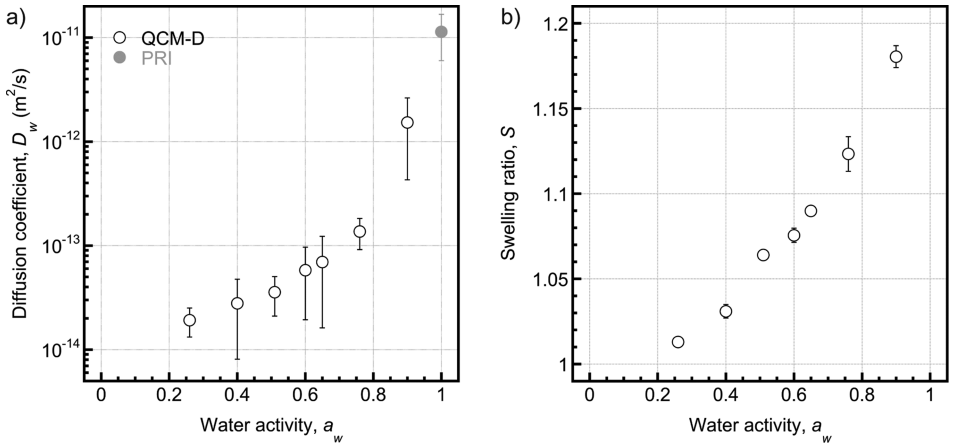

Figure 2. Extrapolation of the transport and swelling properties of the OH-coated PA bilayer as measured by QCM-D. (a) Average apparent water diffusion coefficient of the bilayer as a function of water vapor activity (filled white circles). Error bars indicate the standard deviation from three experiments on three samples. Also included in this plot is the water diffusion coefficient of the bilayer measured by poroelastic relaxation indentation (PRI) (filled gray circle). Note that the PRI experiment is done in liquid water. (b) Average swelling ratio of the bilayer as a function of water vapor activity. Error bars indicate the standard deviation from three experiments on three samples.

ammonia, and deionized (DI) water at 75 °C for 5 min; and finally UV−ozone cleaned for an additional 10 min. Prior to the DMF evaporating, the PSF layer was dissolved off using dichloromethane, leaving the PA−OH bilayer physisorbed to the sensor with the PA layer exposed to atmosphere. Samples were dried overnight in a vacuum. Prior to each experiment, samples were soaked in DI water for 5 min and subsequently dried with dry nitrogen for 10 cycles to minimize potential hysteresis. The thickness and morphology of the PA−OH bilayer was characterized using AFM (Bruker Dimension Icon), showing an average thickness of 164 ±13 nm with a root-mean-square (rms) roughness of 42 ± 3 nm.

Quartz Crystal Microbalance with Dissipation. The QCM-D experiments were conducted with a Q-sense E4 system with flow modules (Biolin Scientific/Q-sense,Västra Frölunda, Sweden) on AZ-cut 5 MHz piezoelectric quartz crystal sensors with gold electrodes (Biolin Scientific, QSX 301). An alternating current applied across the gold electrodes forces the quartz crystal to oscillate in shear at its resonance frequency, which is highly stable and precise due to the material properties of the crystal. QCM-D has a 200 Hz time resolution and nanogram mass sensitivity.

Deposition of the bilayer onto the sensor increases the impedance to oscillation, thereby reducing its resonance frequency and potentially increasing the dissipation (D). For a sample rigidly coupled to the oscillator, the change in resonance frequency, Δf, is directly proportional to the change in the areal mass density, Δm, according to the Sauerbrey relationship given by[29]

$$\Delta m = -\frac{C}{n}\Delta f \tag{2}$$

where C is a proportionality constant (≈17.7 Hz ng/cm^2) that arises from the material properties of the quartz crystal and n is the overtone of the frequency. The validity of this relationship breaks down for materials that are highly viscous or thick.[30] The Sauerbrey relation is valid for the dissipation values of the RO bilayer studied in this work on the basis of a validity threshold of 5×10^{-5}. The actual change in mass, ΔM, from the areal mass density is obtained by multiplying Δm by the lateral area of the bilayer.

Differential Desorption Experiments. The water diffusion coefficient and swelling ratio of the bilayer were characterized using QCM-D as a function of relative humidity (RH) by means of differential desorption experiments. Experiments were performed for different initial RH ranging from 26% RH up to 90% RH using the following procedure. The bilayer was first equilibrated to a desired (initial) RH inside of a flow module with a 20 μL sample chamber at 25 °C via a 0.5 L/min steady stream of humidified nitrogen. Specific relative humidities were obtained by flowing dry nitrogen through aqueous salt solutions. At t = 0, the RH was reduced approximately 15% by switching to another humidified nitrogen stream using a right-angle flow switching valve (IDEX Health & Science, Inc., Oak Harbor, WA). Data were collected for each sorption experiment for at least 30 min. The initial and final RH values were measured during each experiment using a humidity probe (Electro-Tech Systems, Inc., Glenside, PA).

Poroelastic Relaxation Indentation (PRI). PRI was used to validate the water diffusion coefficients measured by QCM-D.[31] PRI is also a gravimetric-based technique that measures transport of a polymer layer submerged in a water reservoir by applying a mechanical deformation to cause a time-dependent deswelling of the polymer. The time scale of deswelling can be used to measure the water diffusion coefficient in the PA bilayer. Details of the PRI approach can be found elsewhere.[31−33]

3. RESULTS AND DISCUSSION

The sorption and swelling can be approximated in the thickness direction (z) for thin bilayers, such as the one studied in this work, where the thickness (h) is much smaller than the in-plane dimensions of the sample. For one-dimensional Fickian diffusion, the change in solvent concentration (c) with respect to time is related to the solvent flux density and diffusion coefficient (D) by Fick's second law of diffusion:[34]

$$\frac{\partial c}{\partial t} = \frac{\partial^2}{\partial z^2}(Dc) \tag{3}$$

If D is independent of concentration, an analytical expression for the change in sorbed mass, $\Delta M(t)$, due to a change in concentration at the sample surface can be obtained from eq 3.[35] The initial change in mass can be approximated as

$$\frac{\Delta M(t)}{\Delta M(\infty)} = \frac{2}{h}\sqrt{\frac{D}{\pi}}\sqrt{t} \tag{4}$$

where $\Delta M(\infty)$ is the total change in mass once the sample has equilibrated. This approximation is typically valid for $\Delta M(t)/\Delta M(\infty) < 0.5$.

For the bilayer studied in this work, there are two considerations for characterizing transport properties via sorption experiments. First, the diffusion coefficient in many polymer−solvent systems is concentration-dependent because of changes in the polymer network structure induced by the

DOI: 10.1021/am507091s
ACS Appl. Mater. Interfaces 2015, 7, 3492−3502

solvent, such as swelling.[36] The OH-coating is expected to be hydrophilic, and PA networks have also been shown to swell up to 15%.[32] To account for the concentration dependence of the diffusion coefficient, differential desorption experiments were performed for a variety of initial RH values. In addition to capturing the concentration dependence of the diffusion coefficient, this helps to minimize the error in using eq 4 in characterizing the initial transport behavior. A second issue is that the transport predicted by eq 4 is for a homogeneous layer. To gain insight into the sorption kinetics for a layered system, we apply a bilayer mass transport model for the boundary conditions present in the QCM-D experiments, which we use to interpret our experimental results.

Representative data from the differential desorption experiments are shown in Figure 1. Figure 1b shows the change in the resonance frequency (Δf) due to a change in the RH and the corresponding change in areal mass density (Δm) according to eq 2. A schematic of the QCM-D sample environment is shown in Figure 1c. Figure 1d shows typical results for the normalized initial decrease in mass for four different initial RH's ranging from 26% to 90%. Using the sample's initial swollen thickness for h, we apply eq 4 to extract an apparent diffusion coefficient with a simple linear fit, the results of which are shown in Figure 2a. To validate the diffusion coefficients measured from QCM-D, the diffusion coefficient of the bilayer in liquid water was measured using poroelastic relaxation indentation (PRI) experiments; this is also shown in Figure 2a at $a_w = 1$ (a_w = % RH/100% RH).

The swelling ratio (S) at a given a_w can be obtained from the ratio of the equilibrium swollen mass [$M(\infty)$] to the dry mass (M_{dry})

$$S = \frac{M(\infty)}{M_{dry}} \tag{5}$$

M_{dry} is obtained from the change in the resonance frequency of the sensor after the bilayer has been deposited at 0% RH. Results for the apparent water diffusion coefficient and swelling ratio versus water vapor activity are shown in parts a and b of Figure 2, respectively.

Figure 2 shows that both the swelling and the apparent water diffusion coefficient of the bilayer increase with increasing water activity, which has been observed in several other solvent–polymer systems.[37−39] Equilibrium swelling is most often described with the Flory–Rehner theory,[40] which describes equilibrium swelling as a balance between the resistance to swelling due to polymer chain stretching and the driving force for swelling according to the Flory–Huggins theory.[40,41] The scaling relationship between the swelling ratio and the activity of the water vapor is commonly used to extrapolate thermodynamic parameters, including the solvent–polymer interaction parameter and the cross-link density of the polymer network.[32,40,41]

The logarithmic increase of the diffusion coefficient with water activity suggests that transport in the polymer–solvent system can be interpreted by the free volume theory of diffusion.[42−44] Generally, the free volume theory states that the diffusion coefficient can be expressed as

$$D \sim \exp\left(-\frac{V^*_{H_2O}}{V^o_f}\right) \tag{6}$$

where $V^*_{H_2O}$ is a characteristic volume required by a water molecule to "jump" or diffuse and V^o_f is the total "free volume" per unit volume of the solvent–polymer system. Free volume (V_f) can be understood as spaces created by fluctuations in the solvent–polymer system that are available to solvent molecules for diffusion. The dependence of the diffusion coefficient on concentration was first formalized by Yasuda et al.,[45] who stated that the free volume is proportional to the volume fraction of water (ϕ) in the solvent–polymer system. Assuming molecular compressibility, the volume fraction of water is related to swelling as

$$\phi = 1 - \frac{1}{S} \tag{7}$$

suggesting that the scaling relationship between diffusion and swelling can be used to extrapolate the characteristic volume ratio critical to solvent transport through the polymer.[45] Characterizing this volume ratio is of particular interest for the dense PA layer, as commercial PA membranes are designed to permit the greatest water flux (as predicted by eq 1) while remaining highly selective against salt ions.

For the PA–OH bilayer, extrapolating these fundamental parameters requires first accounting for the effect of the OH-coating on the sorption data. To do so, we present a Fickian bilayer mass transport model that predicts the time-dependent contribution of each layer to the overall change in mass as a function of the material properties and thickness of each layer. By characterizing the role of each layer in the total sorption, we identify instances where eq 4 can be used to approximate the apparent water diffusion coefficient in the PA layer.

Bilayer Mass Transport Model. The bilayer mass transport model presented here has been used to describe the diffusion of gas and solvent in polymer bilayers.[46,47] Figure 3a shows a schematic of the bilayer configuration in our QCM-D experiments illustrating that the OH-coating is in contact with the impermeable sensor while the PA layer is exposed to the water vapor environment. Cross-sectional TEM images (Figure 3b) indicate that the coating is conformal with the PA selective

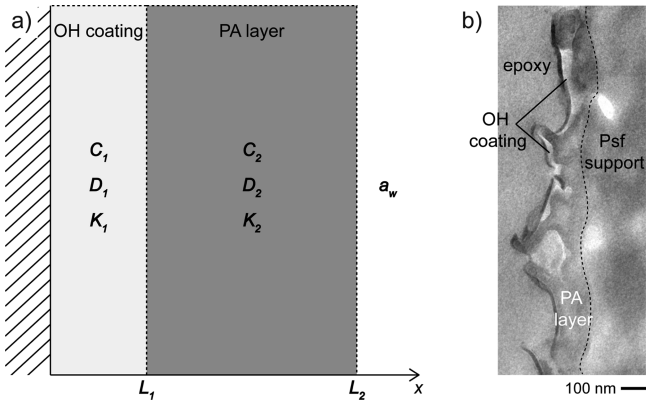

Figure 3. (a) Schematic of the bilayer mass transport model. C_i, D_i, and K_i represent the initial concentration, diffusion coefficient, and solubility within each layer, where $i = 1$ for the OH rich layer and $i = 2$ for the PA selective layer. (b) Transmission electron micrograph (TEM) of the commercial reverse osmosis membrane illustrating the hydroxyl (OH) coating, the polyamide (PA) selective layer, and the polysulfone (PSF) porous support. A thin coat of carbon was used to delineate the OH-coating from the epoxy resin in which the thin-film composite membrane was embedded for TEM sectioning.

DOI: 10.1021/am507091s
ACS Appl. Mater. Interfaces 2015, 7, 3492−3502

layer, which is backed by the PSF support (an additional image in Figure 2 of the SI indicates the contrast between the PA layer and the PSF support). Recent scanning and transmission electron micrography studies of fully aromatic RO membranes formed via an IP technique show that their precise structure consists of a dense core as well as polyamide bubblelike structures,[9,48] which, for the commercial bilayer studied in this work, likely protrude into the OH-coating. We assume that the roughness and inhomogeneities are negligible relative to the length-scale of diffusion and approximate the PA membrane and OH-coating as smooth layers with a constant thickness. The thickness value for each layer is approximated as proportional to the area fraction of each layer in the cross-sectional TEM images.[49] The area fractions were multiplied by the total thickness measured by AFM (≅164 nm) to obtain representative layer thicknesses ≅41 and ≅123 nm for the OH-coating and PA layer, respectively.

The change in water concentration with time in each layer is assumed to obey Fick's second law

$$\frac{\partial c_1}{\partial t} = D_1 \frac{\partial^2 c_1}{\partial z^2} \quad \text{for} \quad 0 \le z \le L_1 \tag{8a}$$

$$\frac{\partial c_2}{\partial t} = D_2 \frac{\partial^2 c_2}{\partial z^2} \quad \text{for} \quad L_1 \le z \le L_2 \tag{8b}$$

where subscript "1" refers to the OH-rich layer, which has thickness L_1, and subscript "2" refers to the PA layer, which has thickness $L_2 - L_1$.

Initially, the water concentration in each layer is constant, as represented by c_{1i} and c_{2i} and defined as

$$c_1(t=0) = c_{1i} \qquad c_2(t=0) = c_{2i} \tag{9}$$

For the configuration shown in Figure 3, we have the following boundary conditions. At $z = 0$ the OH-coating is in contact with the impermeable sensor, so there is zero flux at that interface. At the interface of the two polymers, the flux is equal and the chemical potential of water in the two layers is in equilibrium. The latter requires that the ratio of concentration (c_1, c_2) to solubility (k_1, k_2) within each layer is equal. Similarly, water in the PA layer at $z = L_2$ is in equilibrium with the water vapor above the PA layer (c^*). In summary, for $t > 0$, the boundary conditions are

$$\frac{\partial c_1}{\partial z} = 0 \quad \text{at} \quad z = 0 \tag{10a}$$

$$D_1 \frac{\partial c_1}{\partial z} = D_2 \frac{\partial c_2}{\partial z} \quad \text{at} \quad z = L_1 \tag{10b}$$

$$\frac{c_1}{k_1} = \frac{c_2}{k_2} \quad \text{at} \quad z = L_1 \tag{10c}$$

$$\frac{c_2}{k_2} = c^* \quad \text{at} \quad z = L_2 \tag{10d}$$

The bilayer mass transport problem can be solved by using a method based on the separation of variables originally developed for the analogous problem of heat transfer across two slabs with different material properties.[44] Using this approach we derive the solution for the initial and boundary conditions in eqs 9 and 10, which is provided in full in the Appendix. From this solution, the time-dependent concentration profiles in layers 1 and 2 are given by

$$c_1(z,t) = \sum_{n=1}^{\infty} A_n \sin\left(\lambda_n\left(1 - \frac{L_1}{L_2}\right)\right) \cos\left(\frac{D_1}{D_2 L_2}\lambda_n z\right) \exp\left(-\lambda_n^2 \frac{D_2}{L_2^2} t\right) \quad \text{for} \quad 0 \le z \le L_1 \tag{11a}$$

$$c_2(z,t) = \sum_{n=1}^{\infty} A_n \sin\left(\left(1 - \frac{z}{L_2}\right)\lambda_n\right) \cos\left(\frac{D_1 L_1}{D_2 L_2}\lambda_n\right) \exp\left(-\lambda_n^2 \frac{D_2}{L_2^2} t\right) \quad \text{for} \quad L_1 \le z \le L_2 \tag{11b}$$

where λ_n and A_n are constants that depend on the solubility, diffusion coefficient, and thickness of each layer and are determined by solving eqs A.15 and A.16, respectively. The sorbed mass in each layer is obtained by integrating eqs 11a and 11b as follows:

$$M_1(t) = \int_0^{L_1} c_1(z,t)\, dz \tag{12a}$$

$$M_2(t) = \int_{L_1}^{L_2} c_2(z,t)\, dz \tag{12b}$$

While we are primarily concerned with characterizing transport in the selective PA layer, this model can also provide a qualitative understanding of how the OH-coating affects transport. Because of the proprietary nature of composite desalination membranes, we are unable to characterize the material properties of the individual layers required to solve eqs 11a and 11b. However, we can utilize this model to (1) gain insight into activity-dependent mass transport in a bilayer using heuristic material property values in the limits of low and high RH and (2) identify conditions in which sorption behavior (i.e., effective diffusion coefficients) can be evaluated for individual layers.

The solubility and thickness can be obtained from the activity-dependent swelling ratio of each layer. The one-dimensional swelling ratio is approximately equal to the thickness ratio (neglecting the difference in densities between the two layers results in an error of less than 2% at the highest RH), and the solubility is determined simply as the ratio of the sorbed mass to the dry mass. Due to the underdetermined nature of the QCM-D sorption data for the bilayer, we use a thermodynamic swelling model to estimate the contribution of the PA selective layer to the total swelling ratio. For a model PA membrane with the same network chemistry as the selective PA membrane layer, it has been shown that one-dimensional swelling can be described by the Painter–Shenoy swelling model[32] as

$$\ln a = \ln\left(1 - \frac{1}{S}\right) + \frac{1}{S}\left(1 + \frac{\chi}{S}\right) + \frac{1}{N}\left(\frac{S}{N} - \frac{1}{6S}\right) \tag{13}$$

where $\chi = 0.67 + 0.68/S + 0.71/S^2$ is the Flory–Huggins interaction parameter and $N \cong 3.6$ is the number of monomer units between cross-link junctions for this particular PA network. The swelling ratio of the OH-coating is assumed to be the difference between the swelling ratio from eq 13 and the total swelling ratio of the bilayer from QCM-D.

To approximate diffusion coefficients for each layer, we first consider the qualitative behavior of water diffusion within each layer. From the time-dependent portion of eq 11a, it can be

DOI: 10.1021/am507091s
ACS Appl. Mater. Interfaces 2015, 7, 3492–3502

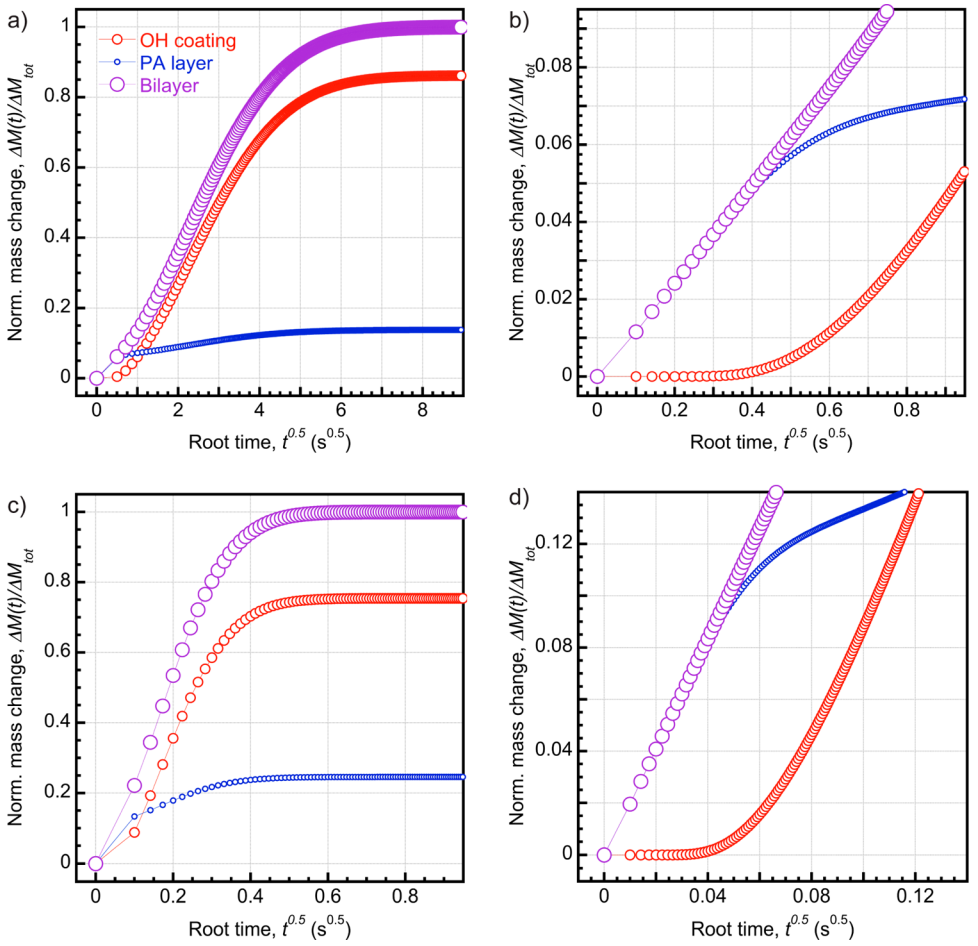

Figure 4. Results from the bilayer mass transport model illustrating the expected desorption behavior within each layer in the limit of high and low RH. Predicted normalized change in mass $\Delta M(t)/\Delta M_{tot}$ versus the square root of time ($t^{1/2}$) for desorption from a_w = 0.2 to 0.05 (a and b) and from a_w = 0.9 to 0.75 (c and d). Both sets of desorption data show that the PA layer dominates the mass change at initial times while the OH-coating dominates the mass change at later times.

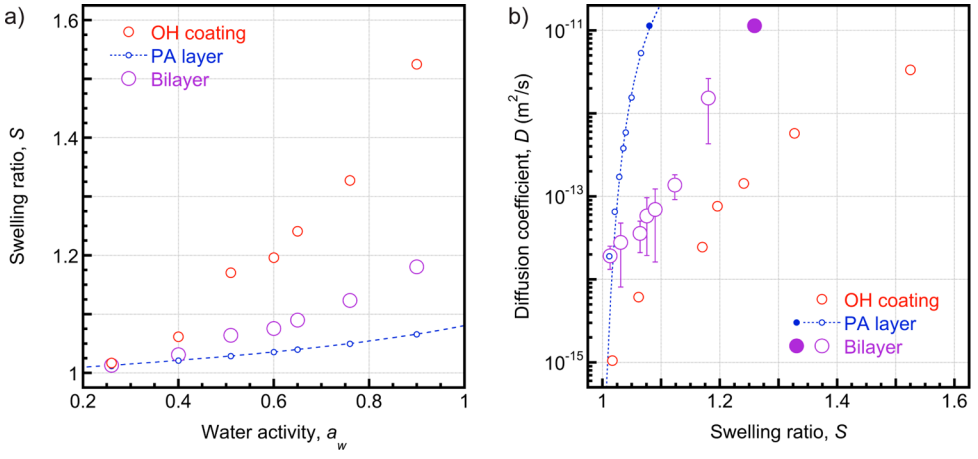

Figure 5. (a) Swelling ratio (S) versus water activity (a_w) of the bilayer, the PA selective layer, and the OH-coating. The curve is a fit of the results for the PA selective layer as defined by eq 13. Note that the OH-coating and the PA layer do not generally experience the same a_w. Instead, the water activity "seen" by the OH-coating ("$a_{w,\,L_1}$") is limited to the water content in the PA layer at the interface, which ranges from $a_{w,\,L_1} \approx 0.01$ to 0.08 for $a_{w,\,L_2} \approx 0.26$–0.90. (b) Water diffusion coefficient, D, for $\Delta M(t)/\Delta M_{tot} < 0.1$ versus swelling ratio for the bilayer, the PA selective layer, and the OH-coating. The dashed line is a fit of results for the PA selective layer as defined by eq 16. Open symbols correspond to the results from QCM-D and closed symbols correspond to the results from PRI. Error bars on the bilayer indicate the standard deviation from three experiments performed on three samples.

DOI: 10.1021/am507091s
ACS Appl. Mater. Interfaces 2015, 7, 3492−3502

seen that the onset of desorption in layer 1 (OH-coating) due to a change in a_w at $z = L_2$ depends on the diffusion coefficient and thickness of layer 2. For example, decreasing D_2 delays the onset of desorption in layer 1. As an upper limit, we use the diffusion coefficients in Figure 2 for the PA layer. For the hydrophilic OH-coating, we expect the diffusion coefficient to be higher. Because the PA layer is a bottleneck for flux, the water diffusion coefficient of layer 1 (the OH-coating) only influences the rate of equilibration within the OH-coating. For simplicity, we assume a constant (and high) value for the diffusion coefficient in layer 1, $D = 5 \times 10^{-10}$ m^2/s, on the basis of reported diffusion coefficients of highly hydrated materials with similar chemical compositions (provided in the SI).

The predicted normalized change in mass in each layer due to a 15% decrease in the RH is shown in Figure 4 for high (0.90) and low (0.20) initial a_w. In both cases, the OH-coating contributes more to the total change in mass due to the high solubility of water in this layer. This suggests that the coating serves as a getter layer or water sink during membrane operation by increasing the water concentration at the PA−OH interface as compared to an uncoated PA surface.

Figure 4b,d shows the initial normalized change in mass at low and high initial water activity, a_w. In both cases, layer 2 determines the initial sorption kinetics up to some normalized change in mass, $\Delta M(t)/\Delta M_{tot}$. This is of interest because before the OH-coating begins contributing to the sorption kinetics, eq 4 can be used to extract the diffusion coefficient of the PA selective layer; beyond this, the apparent diffusion coefficient will be influenced by the transport characteristics of layer 1. At $a_w = 0.9$, layer 2 determines the sorption kinetics up to $\Delta M(t)/\Delta M_{tot} \approx 0.1$, while at $a_w = 0.2$, this is only true up to $\Delta M(t)/\Delta M_{tot} \approx 0.05$. This is due to the increased thickness of the top layer due to swelling. However, due to the increase in the diffusion coefficient of layer 2 at high a_w, the time scale of this regime is significantly shorter. This may explain the deviation of the diffusion coefficients from the logarithmic dependence on water activity below $a_w = 0.5$ in Figure 2a. Thus, we limit the data over which we fit eq 4 to $\Delta M(t)/\Delta M_{tot} < 0.1$ and extrapolate from high a_w to estimate the diffusion coefficients for low a_w. We then estimate the activity-dependent diffusion coefficients of the OH-coating by fitting the bilayer mass transport model to the QCM-D data for each differential desorption experiment. The corrected values are presented in Figure 5b.

While we cannot easily measure the properties of the individual layers in the bilayer, we can compare our results with reported values of water diffusion coefficients in homogeneous PA membranes. A spectroscopic study of liquid water diffusivity in PA membranes fabricated via IP of TMC and MPD (i.e., the same chemistry as the PA membrane in the SWHR membrane) reported effective diffusion coefficients of water between $D = 0.33 \times 10^{-12}$ and 2.20×10^{-12} m^2/s, depending on the amount of carboxylic acid groups present in the membrane.[50,51] Additionally, a PRI study of water transport in PA membranes fabricated with TMC and MPD via molecular layer-by-layer assembly reported a water diffusion coefficient of $D = 3.76 \times 10^{-12}$ m^2/s.[31] At the highest water activity in our study ($a_w = 0.9$) the effective water diffusion coefficient in the PA layer is $D = 5.28 \times 10^{-12}$ m^2/s, which is comparable to the reported values from spectroscopy and PRI.

In Figure 5b, we note that the diffusion coefficients for the OH-coating are low, which may be counterintuitive given the high affinity of hydroxyl-rich polymers toward water. This is primarily due to the fact that the diffusion coefficient is obtained from the short-time solution (eq 4), i.e., over a period during which sorption is occurring predominantly within the PA layer and the sorption kinetics of the OH-coating are low. We also note that the two layers do not generally experience the same a_w. It is intuitive that layer 2 equilibrates to the activity of water in the humidified nitrogen at its surface (i.e., a_w at $z = L_2$). However, the water activity that layer 1 "experiences" is the water content at the interface between layers 1 and 2, which is limited to the solubility of water in layer 2. So, while a_w ranges from 0.26 to 0.90 at $z = L_2$, the range of a_w at $z = L_1$ is only 0.01 to 0.08.

From the intrinsic water permeability (K) of each layer (i.e., the product of the diffusion coefficient and solubility of each layer) it can be seen that the OH-coating is significantly more permeable than the PA membrane. For example, at $a_w = 0.90$, the OH-coating permeability is approximately an order of magnitude greater than the PA layer permeability. This confirms the role of the OH-coating as a getter layer for enhancing the overall water flux of the membrane.

Lastly, we look at the implications of the free volume interpretation of diffusion. Namely, how does network swelling affect the free volume and, in turn, the transport behavior of the PA selective layer? In the dry state, the PA selective layer is a dense, nonporous polymer network with a characteristic free volume, $V_f^o = V_{f,PA}^o$. As mentioned earlier, Yasuda et al.[45] first suggested that the free volume is proportional to the volume fraction of water (ϕ) in a solvent-swollen polymer. As a first approximation, the total free volume of the solvent−polymer system is assumed to be the sum of the free volume contribution of each component[52]

$$V_f^o = \phi V_{f,H_2O}^o + (1 - \phi) V_{f,PA}^o \tag{14}$$

where V_{f,H_2O}^o is the free volume of pure water.

In solution-diffusion theory, water diffusion through the PA layer is based on the probability that the free volume is sufficiently large for passage of water molecules. The diffusion coefficient of water in the swollen PA layer at a given temperature is related to the characteristic jump diffusion volume of a water molecule ($V_{H_2O}^*$),[52]

$$D = D_0 \exp\left(-V_{H_2O}^*\left(\frac{1}{V_f^o} - \frac{1}{V_{f,H_2O}^o}\right)\right) \tag{15}$$

Substituting eqs 7 and 14 into eq 15 yields the following relationship between the water diffusion coefficient and the swelling ratio

$$D = D_0 \exp\left(-\alpha\left(\left(1 - \frac{1}{S} + \frac{\beta}{S}\right)^{-1} - 1\right)\right) \tag{16}$$

where $\alpha = V_{H_2O}^*/V_{f,H_2O}^o$ and $\beta = V_{f,PA}^o/V_{f,H_2O}^o$ are volumetric and free volume ratios, respectively. A best-fit of eq 16 to the water diffusion results for the PA selective layer yields the following fitting parameters: $\alpha = V_{H_2O}^*/V_{f,H_2O}^o = 0.48$ and $\beta = V_{f,PA}^o/V_{f,H_2O}^o = 0.03$ (Figure 5b).

The parameters α and β presented here are considered simply as fitting constants; their physical significance is linked to real free volume parameters that are nontrivial to measure and quantify. Nonetheless, these parameters can be utilized to obtain additional insight into membrane performance. Namely,

DOI: 10.1021/am507091s
ACS Appl. Mater. Interfaces 2015, 7, 3492−3502

in solution-diffusion theory, the volumetric ratio $V^*_{H_2O}/V^o_f$ from eq 6 can be considered a characteristic of the membrane.[52] By rearranging β for $V^o_{f,PA}$ and plugging it into eq 14, the total free volume can be rewritten as

$$V^o_f = \phi V^o_{f,H_2O} + (1-\phi)\alpha V^o_{f,H_2O} = V^o_{f,H_2O}(\phi + \alpha(1-\phi)) \quad (17)$$

Thus, the total free volume of a swollen membrane can be described by V^o_{f,H_2O}, α, and ϕ, which are known[53,54] or measurable quantities. Similarly, $V^*_{H_2O} = \alpha V^o_{f,H_2O}$, so the volumetric ratio from eq 6 can be rewritten as

$$\frac{V^*_{H_2O}}{V^o_f} = \frac{\alpha}{\phi + \alpha(1-\phi)} \quad (18)$$

Thus, the fitting parameters from eq 16 can be used to facilitate comparison of membranes that can be described according to the solution-diffusion model. Measuring these fundamental PA network properties, which determine water swelling and water diffusion, is critical to the understanding of water transport in these materials and the design of next-generation water desalination membranes. Work is currently underway to apply this approach to investigate the relationship between these free volume parameters and various aromatic PA network chemistries that are relevant to desalination membranes.

4. CONCLUSION

In this work, the use of QCM-D for characterizing the transport behavior of the PA selective layer of a commercial RO TFC membrane was demonstrated for water vapor activities ranging from a_w = 0.26 to 0.90.

To account for the effect of the OH-coating on the total mass sorption measured by QCM-D, we implemented a Fickian bilayer mass transport model that identifies the concentration profile in each layer as a function of time. Conclusions from the bilayer mass transport model relevant to the experimental work performed in this study include the following:

(1) The normalized change in mass due to a change in the water vapor activity above the bilayer initially occurs solely within the PA selective layer.

(2) Increasing the thickness or reducing the water diffusion coefficient of the top layer (layer 2) increases the amount of the initial normalized mass uptake, $\Delta M(t)/\Delta M_{tot}$, that can be attributed primarily to the top layer.

(3) Equation 4 can be used to extrapolate the diffusion coefficient of water in the PA selective layer when the change in mass due to the OH-coating is negligible.

(4) When the top layer of the bilayer geometry is the flux bottleneck, sorption experiments can be used to approximate steady-state diffusion in layer 2. Namely, as layer 2 equilibrates, the rate of change of mass of the bilayer is determined by the steady-state diffusion of water through layer 2. This can be appreciated in Figure 4, where, as layer 2 equilibrates, the slope of the normalized change in mass of layer 1 becomes parallel to the slope of the initial change in mass of layer 2. Thus, provided that the equilibration time of layer 1 is sufficiently long relative to the equilibration time of layer 2, traditional sorption techniques can be used to investigate steady-state diffusion in membranes.

We note that the bilayer mass transport model is applicable for any bilayer that can be described by Fickian diffusion and can be applied to concentration-based data (e.g., IR spectroscopy, ellipsometry) as well.

Finally, the solution-diffusion theory for swelling-dependent diffusion yields two volume ratios, $\alpha = V^*_{H_2O}/V^o_{f,H_2O}$ and $\beta = V^o_{f,PA}/V^o_{f,H_2O}$, which were obtained from fitting the swelling-dependent diffusion expression from solution-diffusion theory to the experimental diffusion data for the PA selective layer. While the physical significance of these volume ratios requires further investigation, they can be used to experimentally characterize $V^*_{H_2O}/V^o_f$ in a tractable manner.

APPENDIX A. MATHEMATICAL DERIVATION OF THE SOLUTION TO THE BILAYER MASS TRANSPORT MODEL

We nondimensionalize eqs 8−10 in the following manner:

$$Z = \frac{z}{L_2} \quad T = \frac{D_2}{L_2^2}t \quad L = \frac{L_1}{L_2} \quad D = \frac{D_{w,1}}{D_{w,2}} \quad K = \frac{k_1}{k_2} \quad (A.1)$$

The nondimensionalized concentrations in each layer (i = 1, 2) are

$$C_i = 1 - \frac{c_i}{k_i c^*} \quad (A.2)$$

The governing equations and the associated boundary conditions and initial conditions may be rewritten in a dimensionless form as

$$\frac{\partial C_1}{\partial T} = D\frac{\partial^2 C_1}{\partial Z^2} \quad \text{for} \quad 0 \le Z \le L \quad \text{and} \quad T > 0 \quad (A.3a)$$

$$\frac{\partial C_2}{\partial T} = \frac{\partial^2 C_2}{\partial Z^2} \quad \text{for} \quad L \le Z \le 1 \quad \text{and} \quad T > 0 \quad (A.3b)$$

$$\frac{\partial C_1}{\partial Z} = 0 \quad \text{at} \quad Z = 0 \quad \text{for} \quad T > 0 \quad (A.4a)$$

$$C_1 = C_2$$
$$DK\frac{\partial C_1}{\partial Z} = \frac{\partial C_2}{\partial Z} \quad \text{at} \quad Z = L \quad \text{for} \quad T > 0 \quad (A.4b, A.4c)$$

$$C_2 = 0 \quad \text{at} \quad Z = 1 \quad \text{for} \quad T > 0 \quad (A.4d)$$

$$C_1 = C_{1i}$$
$$C_2 = C_{2i} \quad \text{at} \quad T = 0 \quad \text{for all } Z \quad (A.5a, A.5b)$$

The bilayer mass transport problem is analogous to that of transient heat conduction between two slabs with different thermal properties, for which several analytical treatments exist.[28] A standard approach to solving the heat equation is to use the method of separation of variables. We begin by looking for solutions with the following form:

$$C_i(Z, T) = \zeta_i(Z)\,\tau_i(T) \quad i = 1, 2 \quad (A.6)$$

By substituting eq A.6 into eqs A.3a and A.3b and rearranging them to separate the variables Z and T, it can be seen that both sides must be equal to an arbitrary separation constant, which we denote $-\lambda^2$:

DOI: 10.1021/am507091s
ACS Appl. Mater. Interfaces 2015, 7, 3492−3502

$$\frac{\zeta_i(Z)}{\zeta_i''(Z)} = D\,\frac{\tau_i(T)}{\tau_i'(T)} = -\lambda^2 \tag{A.7}$$

Equation A.7 can also be given as two ordinary differential equations (ODE):

$$\frac{1}{\eta}\frac{Z_i(z)}{Z_i''(z)} = -\lambda^2 \tag{A.8a}$$

$$\frac{G_i(\tau)}{G_i'(\tau)} = -\lambda^2 \tag{A.8b}$$

The solution to the time-dependent ODE for $i = 1, 2$ is

$$\tau_i(T) = A_n e^{-\lambda_n^2 T} \tag{A.9}$$

where A_n are as-yet undetermined coefficients and λ_n are the corresponding eigenvalues.

We can arrange eqs A.8a and A.4a−A.4d to get the following position-dependent Sturm−Liouville eigenvalue system:

$$\xi_i(Z) = -\lambda^2 \xi_i''(Z) \quad \text{for all } Z \tag{A.10}$$

$$\zeta_1' = 0 \quad \text{at} \quad Z = 0 \tag{A.11}$$

$$DK\zeta_1' = \zeta_2' \qquad \zeta_1 = \zeta_2 \quad \text{at} \quad Z = L \tag{A.12a, A.12b}$$

$$\zeta_2 = 1 \quad \text{at} \quad Z = 1 \tag{A.13}$$

Generally, solutions to Sturm−Liouville problems can be represented by a Fourier series, which describes the solution as the superposition of an infinite set of eigensolutions. Thus, to obtain the complete solution (eq A.6), we need to determine the eigenfunctions (ζ_i), the corresponding eigenvalues (λ_n), and finally, the associated Fourier coefficients (A_n).

By applying the boundary and interface conditions in eqs A.11−A.13 to eq A.10, we get the following position-dependent eigenfunctions:

$$H_{i,n}(Z) = \begin{cases} \zeta_1(Z) = \sin((1-L)\lambda_n) \cos(DZ\lambda_n) & \text{for} \quad 0 \le Z \le L \\ \zeta_2(Z) = \sin((1-Z)\lambda_n) \cos(D\lambda_n L) & \text{for} \quad L \le Z \le 1 \end{cases} \tag{A.14}$$

As discussed by Pontrelli and de Monte,[47] the presence of the concentration discontinuity at the polymer interface (eqs A.4b, A.4c) necessitates the use of quasi-orthogonal functions.[55] The eigenfunctions in eq A.14 form an eigenset, $H_{i,n}(Z)$, that is *not* orthogonal from $Z \in (0,1)$. However, a quasi-orthogonal set can be constructed from $H_{i,n}(Z)$ by multiplying each layer's eigenfunction by an orthogonality factor, B_i, specific to that layer. It has been shown that B_1 can be defined as unity without loss of generality by giving the coefficient for the second eigenfunction, B_2, a ratio of material properties of the two layers.[55] For our problem, this is the ratio of the partition coefficients, K. Once the quasi-orthogonal set has been defined, it can be applied to find the Fourier series coefficients, A_n.

We begin by finding the eigenvalues λ_n, which, as usual, are determined by the real solutions to the determinant of the coefficient matrix resulting from the two boundary conditions and two interface conditions:

$$DK\cot((1-L)\lambda_n) - \tan(DL\lambda_n) = 0 \tag{A.15}$$

The roots of eq A.15 are infinite, real, and distinct. Due to the interface condition, however, they are not monotonic and the roots are not generally located exactly between any two adjacent asymptotes. Additionally, the function has an infinite number of singularity points. We determined the eigenvalues using the RootSearch.m package in Mathematica,[56] which utilizes Brent's method for finding roots (and avoiding poles).[57]

Tittle showed that the Fourier coefficients could be found by solving the following equation:[55]

$$A_n \frac{\int_0^L \zeta_{1,0}\zeta_1\,dZ + K\int_L^1 \zeta_{2,0}\zeta_2\,dZ}{\int_0^L \zeta_1^2\,dZ + K\int_L^1 \zeta_1^2\,dZ} \tag{A.16}$$

where $\zeta_{1,0}$ and $\zeta_{2,0}$ represent the (normalized) constant concentration in layers 1 and 2 at $T = 0$, respectively. From eq A.16, we can get the Fourier coefficient, A_n, corresponding to each eigenvalue, λ_n.

With A_n and λ_n, we can now obtain the solution to the bilayer mass transport problem, originally presented in eq A.6, from the sum of solutions for $n = 1, ..., \infty$:

$$C_1(Z, T) = \sum_{n=1}^{\infty} A_n \sin((1-L)\lambda_n)\cos(DZ\lambda_n)e^{-\lambda_n^2 T} \tag{A.17a}$$

$$C_2(Z, T) = \sum_{n=1}^{\infty} A_n \sin((1-Z)\lambda_n)\cos(D\lambda_n z)e^{-\lambda_n^2 T} \tag{A.17b}$$

As with any Fourier series representation of a solution, it is impossible to include an infinite number of terms in practice. In this work, we included 20 terms in the series solution.

■ ASSOCIATED CONTENT

Supporting Information

PM-IRRAS, TEM, AFM, bilayer mass transport model derivation, and a bilayer mass transport model computational code. This material is available free of charge via the Internet at http://pubs.acs.org.

■ AUTHOR INFORMATION

Corresponding Authors

*E.P.C. e-mail: edwin.chan@nist.gov.

*C.M.S. e-mail: chris.stafford@nist.gov.

Author Contributions

All authors contributed to the development of the experimental design, discussion of the results, and preparation of the manuscript. N.K.N. performed experiments, analyzed the data, and developed and wrote the code for the bilayer mass transport model. E.P.C. and N.K.N. developed and applied the free volume description of swelling-dependent diffusion. All authors have given approval to the final version of the manuscript.

Notes

The authors declare no competing financial interest.

■ ACKNOWLEDGMENTS

The authors would like to thank Dow Filmtec (Edina, MN) for kindly providing the commercial RO membrane studied in this work. Additionally, the authors thank Steven D. Hudson for

DOI: 10.1021/am507091s
ACS Appl. Mater. Interfaces 2015, 7, 3492−3502

training and assistance in collecting TEM images of the SWHR TFC membrane. We thank Eric M. Davis for his assistance in PM-IRRAS data collection and interpretation of the bilayer chemical composition. N.K.N. acknowledges the NIST/National Research Council Postdoctoral Fellowship Program for funding. This article, a contribution of the National Institute of Standards and Technology, is not subject to US copyright. Certain equipment and instruments or materials are identified in the paper to adequately specify the experimental details. Such identification does not imply recommendation or endorsement by the National Institute of Standards and Technology, nor does it imply the materials are necessarily the best available for the purpose.

■ ABBREVIATIONS USED

IP = interfacial polymerization
PA = polyamide
PM-IRRAS = polarization modulation infrared reflection adsorption spectroscopy
PSF = polysulfone
PRI = poroelastic relaxation indentation
RH = relative humidity
RO = reverse osmosis
OH = hydroxyl
QCM-D = quartz crystal microbalance with dissipation
TEM = transmission electron microscopy
TFC = thin-film composite

■ REFERENCES

(1) Fritzmann, C.; Löwenberg, J.; Wintgens, T.; Melin, T. State-of-the-Art of Reverse Osmosis Desalination. *Desalination* **2007**, *216*, 1−76.
(2) Greenlee, L. F.; Lawler, D. F.; Freeman, B. D.; Marrot, B.; Moulin, P. Reverse Osmosis Desalination: Water Sources, Technology, and Today's Challenges. *Water Res.* **2009**, *43*, 2317−2348.
(3) Tang, C. Y.; Kwon, Y.-N.; Leckie, J. O. Probing The Nano- and Micro-Scales of Reverse Osmosis Membranes—A Comprehensive Characterization of Physiochemical Properties of Uncoated and Coated Membranes By XPS, TEM, ATR-FTIR, and Streaming Potential Measurements. *J. Membr. Sci.* **2007**, *287*, 146−156.
(4) Zhang, X.; Cahill, D. G.; Coronell, O.; Mariñas, B. J. Absorption of Water in the Active Layer of Reverse Osmosis Membranes. *J. Membr. Sci.* **2009**, *331*, 143−151.
(5) Wijmans, J. G.; Baker, R. W. The Solution-Diffusion Model: A Review. *J. Membr. Sci.* **1995**, *107*, 1−21.
(6) Vogt, B. D.; Lee, H.-J.; Prabhu, V. M.; Delongchamp, D. M.; Lin, E. K.; Wu, W.; Satija, S. K. X-ray and Neutron Reflectivity Measurements of Moisture Transport Through Model Multilayered Barrier Films for Flexible Displays. *J. Appl. Phys.* **2005**, *97*, 114509.
(7) Eisele, N. B.; Frey, S.; Piehler, J.; Görlich, D.; Richter, R. P. Ultrathin Nucleoporin Phenylalanine−Glycine Repeat Films and Their Interaction with Nuclear Transport Receptors. *EMBO Rep.* **2010**, *11*, 366−372.
(8) Rugar, D.; Hansma, P. Atomic Force Microscopy. *Phys. Today* **1990**, *43*, 23−30.
(9) Pacheco, F. A.; Pinnau, I.; Reinhard, M.; Leckie, J. O. Characterization of Isolated Polyamide Thin Films of RO and NF Membranes Using Novel TEM Techniques. *J. Membr. Sci.* **2010**, *358*, 51−59.
(10) Vogt, B. D.; Soles, C. L.; Jones, R. L.; Wang, C.-Y.; Lin, E. K.; Wu, W.; Satija, S. K.; Goldfarb, D. L.; Angelopoulos, M. Interfacial Effects on Moisture Absorption in Thin Polymer Films. *Langmuir* **2004**, *20*, 5285−5290.
(11) Kim, S.; Dura, J. A.; Page, K. A.; Rowe, B. W.; Yager, K. G.; Lee, H.-J.; Soles, C. L. Surface-Induced Nanostructure and Water Transport of Thin Proton-Conducting Polymer Films. *Macromolecules* **2013**, *46*, 5630−5637.
(12) Eastman, S. A.; Kim, S.; Page, K. A.; Rowe, B. W.; Kang, S.; Soles, C. L.; Yager, K. G. Effect of Confinement on Structure, Water Solubility, and Water Transport in Nafion Thin Films. *Macromolecules* **2012**, *45*, 7920−7930.
(13) Papanu, J. S.; Hess, D. W.; Bell, A. T.; Soane, D. S. In Situ Ellipsometry To Monitor Swelling and Dissolution of Thin Polymer Films. *J. Electrochem. Soc.* **1989**, *136*, 1195−1200.
(14) Fan, Z.; Harrison, D. J. Permeability of Glucose and Other Neutral Species Through Recast Perfluorosulfonated Ionomer Films. *Anal. Chem.* **1992**, *64*, 1304−1311.
(15) Balik, C. On the Extraction of Diffusion Coefficients from Gravimetric Data for Sorption of Small Molecules by Polymer Thin Films. *Macromolecules* **1996**, *29*, 3025−3029.
(16) Marx, K. A. Quartz Crystal Microbalance: A Useful Tool for Studying Thin Polymer Films and Complex Biomolecular Systems at the Solution−Surface Interface. *Biomacromolecules* **2003**, *4*, 1099−1120.
(17) Penon, M. G.; Picken, S.; Wübbenhorst, M.; De Vos, G.; Van Turnhout, J. Dielectric Water Sorption Analysis. *Rev. Sci. Instrum.* **2006**, *77*, 115107.
(18) Barreira, S. V. P.; Garcia-Morales, V.; Pereira, C. M.; Manzanares, J. A.; Silva, F. Electrochemical Impedance Spectroscopy of Polyelectrolyte Multilayer Modified Electrodes. *J. Phys. Chem. B* **2004**, *108*, 17973−17982.
(19) Baukh, V.; Huinink, H. P.; Adan, O. C.; Erich, S. J.; Van Der Ven, L. G. NMR Imaging of Water Uptake In Multilayer Polymeric Films: Stressing the Role of Mechanical Stress. *Macromolecules* **2010**, *43*, 3882−3889.
(20) Nguyen, T.; Bentz, D.; Byrd, E. Method for Measuring Water Diffusion in a Coating Applied to a Substrate. *JCT CoatingsTech* **1995**, *67*, 37−46.
(21) Linossier, I.; Gaillard, F.; Romand, M.; Feller, J. Measuring Water Diffusion in Polymer Films on the Substrate by Internal Reflection Fourier Transform Infrared Spectroscopy. *J. Appl. Polym. Sci.* **1997**, *66*, 2465−2473.
(22) Deabate, S.; Fatnassi, R.; Sistat, P.; Huguet, P. In Situ Confocal-Raman Measurement of Water and Methanol Concentration Profiles in Nafion Membrane Under Cross-Transport Conditions. *J. Power Sources* **2008**, *176*, 39−45.
(23) Hajatdoost, S.; Yarwood, J. ATR-FTIR Spectroscopic Studies of the Structure and Permeability of Sulfonated Poly(ether sulfone) Membranes. Part 3—Effects of Sorption and Desorption, and of Annealing. *J. Chem. Soc. Faraday Trans.* **1997**, *93*, 1613−1620.
(24) Bernstein, R.; Kaufman, Y.; Freger, V. *Encyclopedia of Membrane Science And Technology*; Hoek, E. M. V., Tarabara, V. V., Eds.; Wiley & Sons, Inc., 2013; Chapter 2, pp 1−41.
(25) Theisen, L. A.; Martin, S. J.; Hillman, A. R. A Model for the Quartz Crystal Microbalance Frequency Response to Wetting Characteristics of Corrugated Surfaces. *Anal. Chem.* **2004**, *76*, 796−804.
(26) Cadotte, J. E.; King, R. S.; Majerle, R. J.; Petersen, R. J. Interfacial Synthesis in the Preparation of Reverse Osmosis Membranes. *J. Macromol. Sci., Chem.* **1981**, *15*, 727−755.
(27) Cassagneau, T.; Guérin, F.; Fendler, J. H. Preparation and Characterization of Ultrathin Films Layer-by-Layer Self-Assembled from Graphite Oxide Nanoplatelets and Polymers. *Langmuir* **2000**, *16*, 7318−7324.
(28) Chung, J. Y.; Lee, J.-H.; Beers, K. L.; Stafford, C. M. Stiffness, Strength, and Ductility of Nanoscale Thin Films and Membranes: A Combined Wrinkling−Cracking Methodology. *Nano Lett.* **2011**, *11*, 3361−3365.
(29) Sauerbrey, G. Verwendung Von Schwingquarzen Zur Wägung Dünner Schichten Und Zur Mikrowägung. *Z. Für Phys.* **1959**, *155*, 206−222.
(30) Vogt, B. D.; Soles, C. L.; Lee, H.-J.; Lin, E. K.; Wu, W. Moisture Absorption into Ultrathin Hydrophilic Polymer Films on Different Substrate Surfaces. *Polymer* **2005**, *46*, 1635−1642.

DOI: 10.1021/am507091s
ACS Appl. Mater. Interfaces 2015, 7, 3492−3502

(31) Chan, E. P. Deswelling of Ultrathin Molecular Layer-by-Layer Polyamide Water Desalination Membranes. *Soft Matter* **2014**, *10*, 2949−2954.
(32) Chan, E. P.; Young, A. P.; Lee, J.-H.; Chung, J. Y.; Stafford, C. M. Swelling of Ultrathin Crosslinked Polyamide Water Desalination Membranes. *J. Polym. Sci., Part B: Polym. Phys.* **2013**, *51*, 385−391.
(33) Chan, E. P.; Young, A. P.; Lee, J.-H.; Stafford, C. M. Swelling of Ultrathin Molecular Layer-By-Layer Polyamide Water Desalination Membranes. *J. Polym. Sci., Part B: Polym. Phys.* **2013**, *51*, 1647−1655.
(34) Fick, A. Ueber Diffusion. *Ann. Phys.* **1855**, *170*, 59−86.
(35) Crank, J. *The Mathematics of Diffusion*; Clarendon Press: Oxford, UK, 1975.
(36) Vrentas, J. S.; Duda, J. L. Diffusion in Polymer—Solvent Systems. I. Reexamination of The Free-Volume Theory. *J. Polym. Sci. Polym. Phys. Ed.* **1977**, *15*, 403−416.
(37) Kovacs, A. J. Transition Vitreuse Dans Les Polymères Amorphes. Etude Phénoménologique. In *Fortschritte Der Hochpolymeren-Forschung*; Advances in Polymer Science; Springer: Berlin, 1964; Vol. *3/3*, pp 394−507.
(38) Ramani, R.; Ranganathaiah, C. Free-Volume Microprobe Study of Iodine Diffusion in Polymers. *Polym. Int.* **2001**, *50*, 237−248.
(39) Schaetzel, P.; Vauclair, C.; Nguyen, Q. T.; Bouzerar, R. A Simplified Solution−Diffusion Theory in Pervaporation: The Total Solvent Volume Fraction Model. *J. Membr. Sci.* **2004**, *244*, 117−127.
(40) Flory, P. J.; Rehner, J. Statistical Mechanics of Cross-Linked Polymer Networks II. Swelling. *J. Chem. Phys.* **1943**, *11*, 521−526.
(41) Painter, P. C.; Shenoy, S. L. A Simple Model for the Swelling of Polymer Networks. *J. Chem. Phys.* **1993**, *99*, 1409−1418.
(42) Paul, D. Reformulation of the Solution-Diffusion Theory of Reverse Osmosis. *J. Membr. Sci.* **2004**, *241*, 371−386.
(43) Roh, I. J.; Kim, J.-J.; Park, S. Y. Mechanical Properties and Reverse Osmosis Performance of Interfacially Polymerized Polyamide Thin Films. *J. Membr. Sci.* **2002**, *197*, 199−210.
(44) Kotelyanskii, M. J.; Wagner, N. J.; Paulaitis, M. E. Atomistic Simulation of Water and Salt Transport in the Reverse Osmosis Membrane FT-30. *J. Membr. Sci.* **1998**, *139*, 1−16.
(45) Yasuda, H.; Lamaze, C. E.; Ikenberry, L. D. Permeability of Solutes through Hydrated Polymer Membranes. Part I. Diffusion of Sodium Chloride. *Makromol. Chem.* **1968**, *118*, 19−35.
(46) Poulsen, L.; Zebger, I.; Tofte, P.; Klinger, M.; Hassager, O.; Ogilby, P. R. Oxygen Diffusion in Bilayer Polymer Films. *J. Phys. Chem. B* **2003**, *107*, 13885−13891.
(47) Pontrelli, G.; De Monte, F. Mass Diffusion through Two-Layer Porous Media: An Application to the Drug-Eluting Stent. *Int. J. Heat Mass Trans.* **2007**, *50*, 3658−3669.
(48) Yan, H.; Miao, X.; Xu, J.; Pan, G.; Zhang, Y.; Shi, Y.; Guo, M.; Liu, Y. The Porous Structure of the Fully-Aromatic Polyamide Film in Reverse Osmosis Membranes. *J. Membr. Sci.* **2015**, *475*, 504−510.
(49) Schneider, C. A.; Rasband, W. S.; Eliceiri, K. W. NIH Image to Image-J: 25 Years of Image Analysis. *Nat. Methods* **2012**, *9*, 671−675.
(50) De Monte, F. Transient Heat Conduction in One-Dimensional Composite Slab. A "Natural" Analytic Approach. *Int. J. Heat Mass Trans.* **2000**, *43*, 3607−3619.
(51) Jin, Y.; Wang, W.; Su, Z. Spectroscopic Study on Water Diffusion in Aromatic Polyamide Thin Film. *J. Membr. Sci.* **2011**, *379*, 121−130.
(52) Yasuda, H.; Lamaze, C. E.; Peterlin, A. Diffusive and Hydraulic Permeabilities of Water in Water-Swollen Polymer Membranes. *J. Polym. Sci. Part A-2: Polym. Phys.* **1971**, *9*, 1117−1131.
(53) Stearn, A. E.; Eyring, H. The Deduction of Reaction Mechanisms from the Theory of Absolute Rates. *J. Chem. Phys.* **1937**, *5*, 113−124.
(54) Amzel, L. M. Loss of Translational Entropy in Binding, Folding, and Catalysis. *Proteins Struct. Funct. Genet.* **1997**, *28*, 144−149.
(55) Tittle, C. W. Boundary Value Problems in Composite Media: Quasi-Orthogonal Functions. *J. Appl. Phys.* **1965**, *36*, 1486−1488.
(56) *Mathematica*, Version 9.0; Wolfram Research, Inc.: Champaign, IL.
(57) Brent, R. P. *Algorithms for Minimization Without Derivatives*; Dover Books on Mathematics; Dover Publications: Mineola, NY, 1973.

DOI: 10.1021/am507091s
ACS Appl. Mater. Interfaces 2015, 7, 3492−3502